Peak Power Handling Capability in Groove Gap Waveguide Filters Based on Horizontally Polarized Resonators and Enhancement Solutions

Aitor Morales-Hernández, *Graduate Student Member, IEEE*, Miguel Á. Sánchez-Soriano, *Senior Member, IEEE*, Miguel Ferrando-Rocher, *Member, IEEE*, Stephan Marini, *Senior Member, IEEE*, Máriam Taroncher Calduch, and Vicente E. Boria, *Fellow, IEEE*

***Abstract*— This letter studies the peak power handling capability (PPHC) in groove gap waveguide filters based on horizontally polarized resonators. Moreover, a modification of the resonant cavity is proposed, where the central pins of the original structure are replaced by a rounded metal block. As a result of this change, the TE_{101}-like mode can still be excited, but the maximum electric field strength is shifted to the center of the cavity, which leads to a higher PPHC. The main advantages of the original structure are maintained, and greater robustness in the manufacturing process is achieved. Next, some guidelines for the design of the coupling windows and the dimensions of the blocks are shown to minimize the electric field strength and, consequently, maximize the PPHC. Finally, two third-order bandpass filters (with pins and with blocks) centered at 16 GHz have been manufactured and tested in a measurement campaign, where a PPHC enhancement of 8.7 dB at high pressures is achieved for the novel solution presented in this work.**

***Index Terms*— Corona breakdown, gas discharge, groove gap waveguide (GGW), millimeter-wave filter, peak power handling capability (PPHC).**

I. Introduction

THE ever-increasing demand of new emerging applications where the RF/microwave power requirements are very demanding (for instance, at the output stages of ground and satellite communication systems [1], [2]) makes necessary the study of several power issues, such as the corona breakdown [3], [4]. The analysis of this phenomenon has become an essential step for the design of high peak power handling capability (PPHC) microwave devices working from cm- and mm-waves to even terahertz. This physical effect, also commonly known as the gas breakdown phenomenon, can occur in air-filled components that are subjected to high-strength electric fields. Therefore, if the signal peak power applied to the device is too high, an electrical discharge can take place in the surrounding air, which can lead to a degradation of the performance of the device or even to permanent damage of the component. In this way, some studies have predicted the gas breakdown effect in waveguide devices [5]–[8]. Furthermore, other investigations are focused on analyzing the corona breakdown effect in planar technology [9], [10] and also on proposing some design strategies to improve PPHC in microstrip bandpass filters (BPFs) [11]–[13].

Over the last few years, gap waveguide (GW) technology has been introduced [14], and several structure families (i.e., groove GW (GGW) [15], ridge GW (RGW) [16], and microstrip GW (MGW) [17]) have been presented for the design of multiple microwave components. GWs have become a good alternative to rectangular waveguides (RWs), especially for mm-wave devices, due to the possibility of avoiding the problem of nonperfect metal contact of the involved fabricated pieces.

In particular, among the many GW components that can be found in the literature, filters are one of the most investigated due to their fundamental use in any RF front-end. Different topologies of GW filters have been proposed, such as the ones based on inductive irises [19]–[21], capacitive irises [22], or coaxial resonators [23]. Moreover, a novel horizontally polarized cavity has been proposed in [18] for the design of BPFs, where several advantages are introduced with respect to other previous configurations. This recent structure allows a simple way to implement a bandpass or bandstop filter behavior by the engraving of the resonant cavities on the top or bottom metal plates of GW structures. Some of its attractive features are the flexibility of implementing BPFs at different frequencies by using a common pin plate or the possibility to easily generate a transmission zero (TZ) at the desired frequency. In this work, we first analyze the corona breakdown effect in BPFs based on the previously described topology. Next, a modification of the resonant structure is proposed to reach a PPHC improvement and greater robustness in the manufacturing process of this type of filter without losing any of the advantages described above.

II. Analysis of the Modified Resonant Structure

On the one hand, the resonant structure described in more detail in [18] is shown in Fig. 1(a). One can easily see that the cavity is engraved on the top metal plate (represented by red lines), while, on the bottom metal plate, the periodic

Manuscript received November 15, 2021; revised January 14, 2022; accepted February 21, 2022. This work was supported in part by the University of Alicante through the Fellowship Grant UAFPU2018-054 and in part by MCIN/AEI/10.13039/501100011033 through the Sub-Projects C41 and C43 of the Coordinated Project under Grant PID2019-103982RB. *(Corresponding author: Aitor Morales-Hernández.)*

Aitor Morales-Hernández, Miguel Á. Sánchez-Soriano, Miguel Ferrando-Rocher, and Stephan Marini are with the Department of Physics, Systems Engineering and Signal Theory, University of Alicante, 03690 Alicante, Spain (e-mail: aitor.morales@ua.es; miguel.sanchez.soriano@ua.es; miguel.ferrando@ua.es; smarini@ua.es).

Máriam Taroncher Calduch is with the Val Space Consortium, Ciudad Politécnica de la Innovación, 46022 Valencia, Spain.

Vicente E. Boria is with iTEAM, Universitat Politècnica de València, 46022 Valencia, Spain.

Color versions of one or more figures in this letter are available at https://doi.org/10.1109/LMWC.2022.3154060.

Digital Object Identifier 10.1109/LMWC.2022.3154060

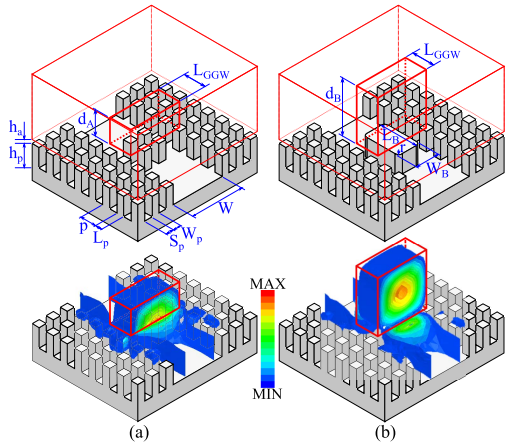

Fig. 1. Resonant cavity structure and electric field distribution. (a) Design presented in [18]. (b) Design proposed in this work.

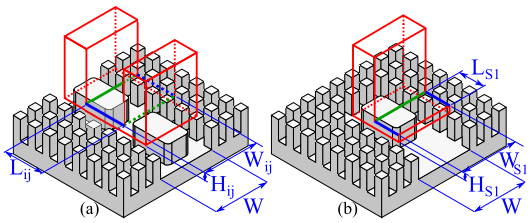

Fig. 2. Coupling design. (a) Intercavity coupling. (b) Input/output coupling.

structure of the bed of nails is extended below the resonant cavity section. By using this topology, a TE_{101}-like mode can be excited horizontally at the resonant frequency f_{101}, as shown in Fig. 1(a), with the representation of the electric field distribution. It is easy to see that, in this case, the resonant mode fields are also located in the air holes between pins. On the other hand, the design strategy proposed in this letter is represented in Fig. 1(b), where, as it can be seen, the cavity is also located on the top plate. However, the four central pins of the bottom metal plate are replaced by a unique metal block, in which the corners have also been rounded with a radius r in order to avoid the sharp edges, where high electric fields can appear (see [12], [24]). By making this change, the TE_{101}-like mode can still be excited, and the maximum electric field can be reduced and shifted to the center of the cavity, as shown in Fig. 1(b). The latter effect occurs because the top face of the block acts as a perfect electric conductor (PEC), and hence, the electric field cannot pass through it. Note that the depth d_B of the cavity (see Fig. 1) must be modified to adjust the resonant frequency f_{101}, where $d_B + h_a \approx d_A + h_a + h_p \approx \lambda_g/2$.

Therefore, the main difference of the electric field ($|\vec{E}|$) distribution between both designs is clearly shown in Fig. 1, where the same scale has been applied for both designs. Taking into account this fact, and knowing its close relationship with the corona discharge breakdown, we could expect that the PPHC will be enhanced for the design proposed in Fig. 1(b). Thus, some guidelines for maximizing the PPHC (through the reduction of the maximum electric field strength) in BPFs based on the proposed structure are described in what follows.

A. Design of the Intercavity and Input (Output) Couplings

In Fig. 2, one can see that three parameters (i.e., width W_{ij}, length L_{ij}, and height H_{ij}) can be used to control the intercavity coupling M_{ij} [see Fig. 2(a)] and other three

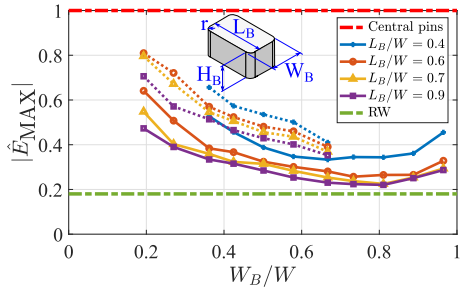

Fig. 3. Study of $|\hat{E}_{MAX}|$ as a function of L_B and W_B. Values have been normalized with respect to the equivalent BPF designed by using four central pins below the cavities. Solid lines are used for blocks with rounded corners ($r = 0.94$ mm), while dotted lines represent nonrounded blocks ($r = \infty$).

parameters (i.e., W_{S1}, L_{S1}, and H_{S1}) to adjust the input (and output) coupling M_{S1} [see Fig. 2(b)]. However, in [18], only the widths of both coupling windows are modified, while the heights and lengths are fixed. In this work, it has been verified that, for maximizing the PPHC of the filter, it is advisable to set the dimensions $W_{ij} = W_{S1} = W$ (where W is the width of the waveguide propagation section) to avoid high $|\vec{E}|$ on the lateral edges of the coupling cavities (plotted in blue in Fig. 2). After that, the parameters H_{ij} (H_{S1}) and L_{ij} (L_{S1}) can be modified to adjust M_{ij} (M_{S1}). Finally, it is also desirable, as far as possible, to minimize the parameters H_{ij} and H_{S1} to avoid a high concentration of $|\vec{E}|$ at the edges located near the center of the cavity (plotted in green in Fig. 2) because, as it has been checked, PPHC may also be lower.

B. Design of the Metal Block Dimensions (W_B, L_B, and H_B)

After providing the previous recommendations, an analysis of the electric field variation as a function of the width and length of the metal block (called W_B and L_B, respectively, as shown in Fig. 3) has been carried out. For this study, several third-order BPFs (as shown, by way of illustration, in Fig. 4) have been designed and simulated by using ANSYS high-frequency structure simulator (HFSS) [25] for multiple combinations of W_B and L_B. For all cases plotted in Fig. 3 (including the prototype based on central pins), the same electrical response is maintained, where the center frequency f_0 is equal to 16 GHz and the fractional bandwidth is 2%. Furthermore, all the prototypes have an ideal Chebyshev response with 20 dB return loss, and the previous guidelines have been taken into account for the design of all the intercavity and Input/output couplings. In Fig. 3, the variation of the maximum normalized electric field strength ($|\hat{E}_{MAX}|$) is plotted as a function of the ratio W_B/W (where $W = 12.954$ mm is the width of a standard WR-51), and different colors are used to represent several lengths of L_B/W, as it is specified in the legend. Moreover, a red dashed line represents $|\hat{E}_{MAX}|$ of an equivalent BPF designed by using four rounded central pins below the cavities, while a dashed green line shows the maximum normalized electric field of the counterpart RW BPF with inductive irises [2], [26] (which is considered the minimum theoretical $|\hat{E}_{MAX}|$ limit). First, as it can be observed, the GW design suggested in this work reaches in all cases lower values of $|\hat{E}_{MAX}|$ than the strategy proposed in [18]. Furthermore, it is similar to that expected for the RW filter when the ratio W_B/W is about 65%–80% and $L_B/W = 90\%$. At this point, it must also be emphasized that it is needed to keep in mind the possible appearance of

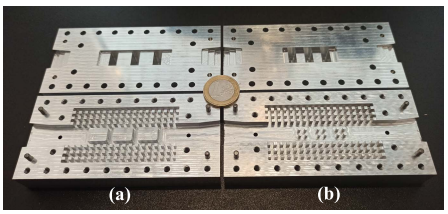

Fig. 4. Photograph of the manufactured prototypes ($W_p = L_p = 1.9$ mm, $h_p = 3.8$ mm, $h_a = 0.2$ mm, $p = 3.8$ mm, and $L_{GGW} = 5.7$ mm; see Fig. 1). Transitions from WR-62 to WR-51 have been included. (a) Proposed design ($L_B = 11.5$ mm, $W_B = 8.6$ mm, and $H_B = 3.4$ mm). (b) Benchmark.

spurious modes and the reduction of the rejection band of the filter for nonoptimal dimensions of W_B and L_B. In addition, the $|\hat{E}_{MAX}|$ values for some combinations of W_B and L_B when the corners of the blocks are not rounded ($r = \infty$) are also plotted in Fig. 3 by using dotted lines. It is easy to observe the importance of avoiding sharp edges to reach higher PPHCs.

Finally, regarding the height of the metal block (named H_B in Fig. 3), it is important to underline that, as occurs in [18] with the height of the central pins, it can be set to the same size as the lateral pins of the GW structure ($H_B = h_p$). However, for narrow air gap values (h_a), it is necessary to slightly decrease H_B in order to allow the coupling of the electromagnetic field to the cavity. As it has been verified, this minor modification does not affect the variation of the PPHC.

III. Implementation and Experimental Results

In view of the above results, a BPF with metal blocks has been manufactured in aluminum with the electrical specifications detailed in Section II-B in order to validate the proposed structure, as can be seen in Fig. 4(a). Furthermore, another BPF (called benchmark), where the resonant structure based on pins has been used, has also been manufactured [see Fig. 4(b)]. Please note that the central pins of the benchmark filter have also been rounded ($r = 0.94$ mm) in order to make a fair comparison between prototypes. The frequency responses and the group delay of both filters have been measured and represented in Fig. 5. Note that a drawback of the suggested strategy is the increased size and weight of the prototype due to the longer height (d_B) of the cavities. However, greater robustness of the structure is achieved compared to the benchmark design since the filter performance is very sensitive to the dimensions of the groups of central pins of Fig. 4(b) (which are located inside the cavities of the benchmark prototype, thus acting as perturbations of the TE_{101}-like mode). In fact, a metrology study has also been carried out to verify this point. As shown in Fig. 5, the measured return and insertion losses are 12.1 and 0.65 dB, respectively, for the benchmark prototype, while 21.2 and 0.53 dB are achieved, respectively, for the proposed design. Finally, it is important to highlight that, as previously stated, the proposed resonant structure does not lose any of the advantages presented in [18]. For that reason, another filter was designed at $f_0 = 14$ GHz, where the same bottom plate with blocks, as shown in Fig. 5(a), is maintained, and only the engraved cavities of the top plate are changed. The simulated S-parameters of this filter are also plotted in the inset of Fig. 5 in purple.

A measurement campaign has been carried out at the European High-Power RF Space Laboratory (Valencia, Spain) to validate the breakdown power enhancement. A pulsed signal with a carrier frequency at 15.98 GHz (which corresponds

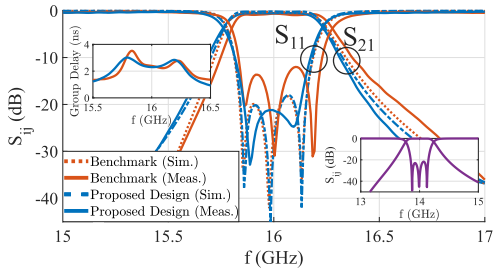

Fig. 5. Simulated and measured frequency responses of both filters.

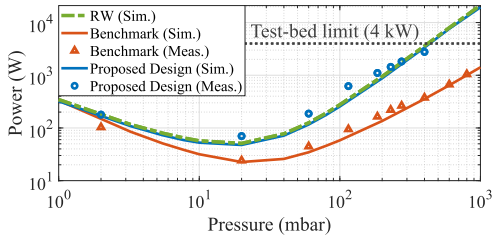

Fig. 6. Simulated and measured corona discharge thresholds (Paschen curves). The simulated values have been obtained by using SPARK3D [27].

to the measured center frequency of both prototypes), low duty cycle (2%), and low width (20 μs) has been used in order to avoid any self-heating effect in the devices under test. The maximum applied signal power of the testbed is 4 kW. The two filters have been measured at 22 °C in a pressured controlled chamber from 2 to 1013 mbar in order to obtain their respective Paschen curves. Different detection methods have been used to identify the corona discharge, as detailed in [10]–[12], where similar measurement campaigns were carried out for microstrip BPFs.

In Fig. 6, the simulated and measured peak power limits for both filters have been plotted. Furthermore, a dashed green line shows the simulated Paschen curve of the counterpart RW filter with inductive irises. One can easily see that, for the filter with the proposed design, the simulated and measured PPHC improvements at high pressures (above 400 mbar) with respect to the benchmark prototype are 10.1 and 8.7 dB, respectively.

IV. Conclusion

In this letter, the corona discharge breakdown of GGW filters based on horizontally polarized resonators has been studied, and a modification of the original resonant cavity has been proposed to improve their peak power limits. It has been verified that the maximum electric field strength can be easily decreased by replacing the original central pins with a metal block since the maximum of the TE_{101}-like mode is shifted to the center of the cavity. Moreover, some recommendations to properly design the coupling windows and the dimensions of the metal blocks have been given for maximizing the corona discharge thresholds. Finally, a measurement campaign has validated the proposed design, showing a PPHC improvement of 8.7 dB compared to the benchmark prototype in the high-pressure range (above 400 mbar), where greater robustness in the manufacturing process is also achieved while maintaining the advantages of the original design.

Acknowledgment

The authors would like to thank Val Space Consortium (VSC) for its contribution—Laboratories funded by the European Regional Development Fund—A way of making Europe.

REFERENCES

[1] M. Yu, "Power-handling capability for RF filters," *IEEE Microw. Mag.*, vol. 8, no. 5, pp. 88–97, Oct. 2007.

[2] R. J. Cameron, C. M. Kudsia, and R. R. Mansour, *Microwave Filters for Communication Systems: Fundamentals, Design, and Applications*, 2nd ed. Hoboken, NJ, USA: Wiley, 2018.

[3] A. D. MacDonald, *Microwave Breakdown in Gases*. New York, NY, USA: Wiley, 1966.

[4] Y. P. Raizer, *Gas Discharge Physics*. Berlin, Germany: Springer, 1991.

[5] C. Ernst and V. Postoyalko, "Prediction of peak internal fields in direct-coupled-cavity filters," *IEEE Trans. Microw. Theory Techn.*, vol. 51, no. 1, pp. 64–73, Jan. 2003.

[6] C. Vicente, M. Mattes, D. Wolk, B. Mottet, H. Hartnagel, J. Mosig, and D. Raboso, "Microwave breakdown prediction in rectangular waveguide based components," in *Proc. German Microw. Conf.*, 2005, pp. 17–20.

[7] T. Pinheiro-Ortega *et al.*, "Microwave corona breakdown prediction in arbitrarily-shaped waveguide based filters," *IEEE Microw. Wireless Compon. Lett.*, vol. 20, no. 4, pp. 214–216, Apr. 2010.

[8] A. Morales-Hernandez, M. Ferrando-Rocher, M. A. Sanchez-Soriano, S. Marini, and V. E. Boria, "Design strategy and considerations to improve corona discharge breakdown in groove gap waveguides," in *Proc. 15th Eur. Conf. Antennas Propag. (EuCAP)*, Mar. 2021, pp. 1–5.

[9] F. J. Pérez-Soler *et al.*, "Rigorous investigation of RF breakdown effects in high power microstrip passive circuits," in *IEEE MTT-S Int. Microw. Symp. Dig.*, Jun. 2009, pp. 833–836.

[10] M. A. Sanchez-Soriano *et al.*, "Peak and average power handling capability of microstrip filters," *IEEE Trans. Microw. Theory Techn.*, vol. 67, no. 8, pp. 3436–3448, Aug. 2019.

[11] A. Morales-Hernández *et al.*, "Enhancement of corona discharge thresholds in microstrip bandpass filters by using cover-ended resonators," *Int. J. Microw. Wireless Technol.*, vol. 13, no. 7, pp. 708–718, Sep. 2021.

[12] A. Morales-Hernandez, M. A. Sanchez-Soriano, S. Marini, V. E. Boria, and M. Guglielmi, "Increasing peak power handling in microstrip bandpass filters by using rounded-end resonators," *IEEE Microw. Wireless Compon. Lett.*, vol. 31, no. 3, pp. 237–240, Mar. 2021.

[13] A. Morales-Hernandez, M. A. Sanchez-Soriano, S. Marini, V. E. Boria, and M. Guglielmi, "Cover-ended resonators to increase corona discharge thresholds in microstrip bandpass filters," in *Proc. 50th Eur. Microw. Conf. (EuMC)*, Jan. 2021, pp. 882–885.

[14] P.-S. Kildal, E. Alfonso, A. Valero-Nogueira, and E. Rajo-Iglesias, "Local metamaterial-based waveguides in gaps between parallel metal plates," *IEEE Antennas Wireless Propag. Lett.*, vol. 8, pp. 84–87, 2009.

[15] M. Ferrando-Rocher, A. Valero-Nogueira, J. I. Herranz-Herruzo, A. Berenguer, and B. and Bernardo-Clemente, "Groove gap waveguides: A contactless solution for multilayer slotted-waveguide array antenna assembly," in *Proc. 10th Eur. Conf. Antennas Propag. (EuCAP)*, Apr. 2016, pp. 1–4.

[16] P.-S. Kildal, A. U. Zaman, E. Rajo-Iglesias, E. Alfonso, and A. Valero-Nogueira, "Design and experimental verification of ridge gap waveguide in bed of nails for parallel-plate mode suppression," *IET Microw., Antennas Propag.*, vol. 5, no. 3, p. 262, Feb. 2011.

[17] A. A. Brazález, E. Rajo-Iglesias, J. L. Vázquez-Roy, A. Vosoogh, and P.-S. Kildal, "Design and validation of microstrip gap waveguides and their transitions to rectangular waveguide, for millimeter-wave applications," *IEEE Trans. Microw. Theory Techn.*, vol. 63, no. 12, pp. 4035–4050, Dec. 2015.

[18] M. Rezaee and A. U. Zaman, "Groove gap waveguide filter based on horizontally polarized resonators for V-Band applications," *IEEE Trans. Microw. Theory Techn.*, vol. 68, no. 7, pp. 2601–2609, Jul. 2020.

[19] A. del Olmo-Olmeda, M. Baquero-Escudero, V. E. Boria-Esbert, A. Valero-Nogueira, and A. J. Berenguer-Verdú, "A novel band-pass filter topology for millimeter-wave applications based on the groove gap waveguide," in *IEEE MTT-S Int. Microw. Symp. Dig.*, Jun. 2013, pp. 1–4.

[20] A. Berenguer, M. Baquero-Escudero, D. Sanchez-Escuderos, B. Bernardo-Clemente, and V. E. Boria-Esbert, "Low insertion loss 61 GHz narrow-band filter implemented with groove gap waveguides," in *Proc. 44th Eur. Microw. Conf.*, Oct. 2014, pp. 191–194.

[21] M. Rezaee, A. U. Zaman, and P.-S. Kildal, "A groove gap waveguide iris filter for V-band application," in *Proc. 23rd Iranian Conf. Electr. Eng.*, May 2015, pp. 462–465.

[22] M. Rezaee and A. U. Zaman, "Capacitive-coupled groove gap waveguide filter," in *Proc. 12th Eur. Conf. Antennas Propag. (EuCAP)*, 2018, pp. 1–5.

[23] M. Baquero-Escudero, A. Valero-Nogueira, M. Ferrando-Rocher, B. Bernardo-Clemente, and V. E. Boria-Esbert, "Compact combline filter embedded in a bed of nails," *IEEE Trans. Microw. Theory Techn.*, vol. 67, no. 4, pp. 1461–1471, Apr. 2019.

[24] S. Sirci *et al.*, "Design and multiphysics analysis of direct and cross-coupled SIW combline filters using electric and magnetic couplings," *IEEE Trans. Microw. Theory Techn.*, vol. 63, no. 12, pp. 4341–4354, Dec. 2015.

[25] *HFSS, Copyright 2021 ANSYS, Inc. All Rights Reserved*. Accessed: 2021. [Online]. Available: https://www.ansys.com/products/electronics/ansys-hfss

[26] V. E. Boria and B. Gimeno, "Waveguide filters for satellites," *IEEE Microw. Mag.*, vol. 8, no. 5, pp. 60–70, Oct. 2007.

[27] *SPARK3D, Copyright 2021 Dassault Systémes*. Accessed: 2021. [Online]. Available: https://www.3ds.com/products-services/simulia/products/spark3d/